NANO LETTERS

LETTER

pubs.acs.org/NanoLett

Frequency-Selective Rotation of Two-Particle Nanoactuators for Rapid and Sensitive Detection of Biomolecules

Andrea Ranzoni,[†,‡] Jean J. H. B. Schleipen,[†] Leo J. van IJzendoorn,[‡] and Menno W. J. Prins*[,†,‡]

[†]Philips Research, High Tech Campus, Eindhoven, The Netherlands

[‡]Eindhoven University of Technology, Department of Applied Physics, Eindhoven, The Netherlands

Supporting Information

ABSTRACT: We describe an optomagnetic bionanotechnology for rapidand sensitive solution-based affinity assays. Nanoactuators made from bioactive magnetic nanoparticles undergo rotational motion in the volume of a fluid under frequency-controlled magnetic actuation. The nanoactuators show a time-dependent scattering cross-section to an incoming light beam. We demonstrate that the temporal behavior of the scattered light intensity relates to the number, the magnetic properties and the size distribution of the nanoactuators, independently revealing the average value and variation in the magnetic properties of the nanoparticles as well as the concentration of nanoactuators. The method is applied to detect biomolecules in fluid by interparticle binding. In a total assay time of less than 3 min, we demonstrate a limit of detection lower than 400 fM in buffer and 5 pM in human plasma.

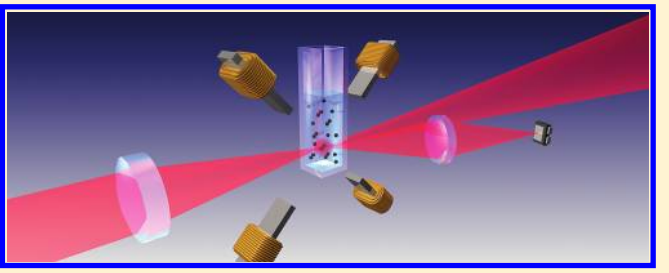

KEYWORDS: Magnetic nanoparticle, rotation, optical scattering, cluster, biosensor

The need for pervasive healthcare drives the field of in vitro diagnostics toward point-of-care solutions to detect biomolecules.[1−5] The technological requirements are very demanding, since point-of-care testing needs to be as reliable and quantitative as testing in a centralized laboratory and at the same time a faster response is required (in the order of a few minutes) in a cost-effective, portable, and integrated detection platform that operates on a small sample volume.[6]

Affinity assays make use of biological molecules to capture specific target molecules from a sample and allow a determination of their concentration. Affinity capture is very effectively achieved by dispersing nano- or microparticles coated with capture molecules into a sample volume.[7−9] Rapid and efficient capture results from the high surface-to-volume ratio of the particles and the high effective concentration of capture molecules in the fluid volume. Ideally, the volume-based capture process is directly followed by a volume-based detection of the captured target molecules. However, it is very challenging to conceive a solution-based detection principle that is very sensitive and specific and that does not intrinsically suffer from large background signals from the volume that is probed.

For a few years now, superparamagnetic particles have been investigated for a novel generation of all-volume-based assays. In the volume of the fluid, magnetic particles capture target molecules and the formation of target-induced clusters of particles is detected. Baudry et al.[10] have demonstrated that a magnetically induced arrangement of nanoparticles in chains results in a very rapid formation of target-induced nanoparticle clusters, which they quantified by a decrease of the optical transmittance of the sample. Other groups measured cluster formation by the reduction of thermal nanoparticle diffusion,[11] by monitoring the growth of long chain lengths,[12] or by a relative change of the transverse relaxation time (T_2) in nuclear magnetic resonance.[13] All these reported physical measurement principles have in common is that they are not intrinsically selective to two-particle clusters with respect to single particles. Single particles already generate a large baseline signal and changes with respect to the baseline quantify the presence of two-particle clusters. The fact that a small change of signal is measured on a large background limits the ability to resolve few particle clusters in the midst of a high number of single nanoparticles and thereby also limits the sensitivity and rapidity of the assays.

In this Letter, we demonstrate a novel technique to selectively actuate, characterize, and detect clusters of magnetic nanoparticles, so-called nanoactuators, within an all-volume-based biological assay. The experimental arrangement is sketched in Figure 1. A laser beam collimated along the *z*-axis illuminates a glass cuvette. Four electromagnets induce a rotating magnetic field inside the cuvette, which causes the magnetic nanoactuators to rotate in the *xz*-plane. A photodetector collects light that is scattered along an angle of approximately 30° from the *z*-axis. Figure 1b describes the different phases of the assay. A short incubation, allowing efficient capture of the target proteins, is followed by the application of a magnetic field to induce chain formation. In the chains, the nanoparticles interact and rapidly form internanoparticle bonds via the captured target molecules. Thereafter the field is removed to allow the chains to

Received: February 1, 2011
Revised: March 1, 2011
Published: March 30, 2011

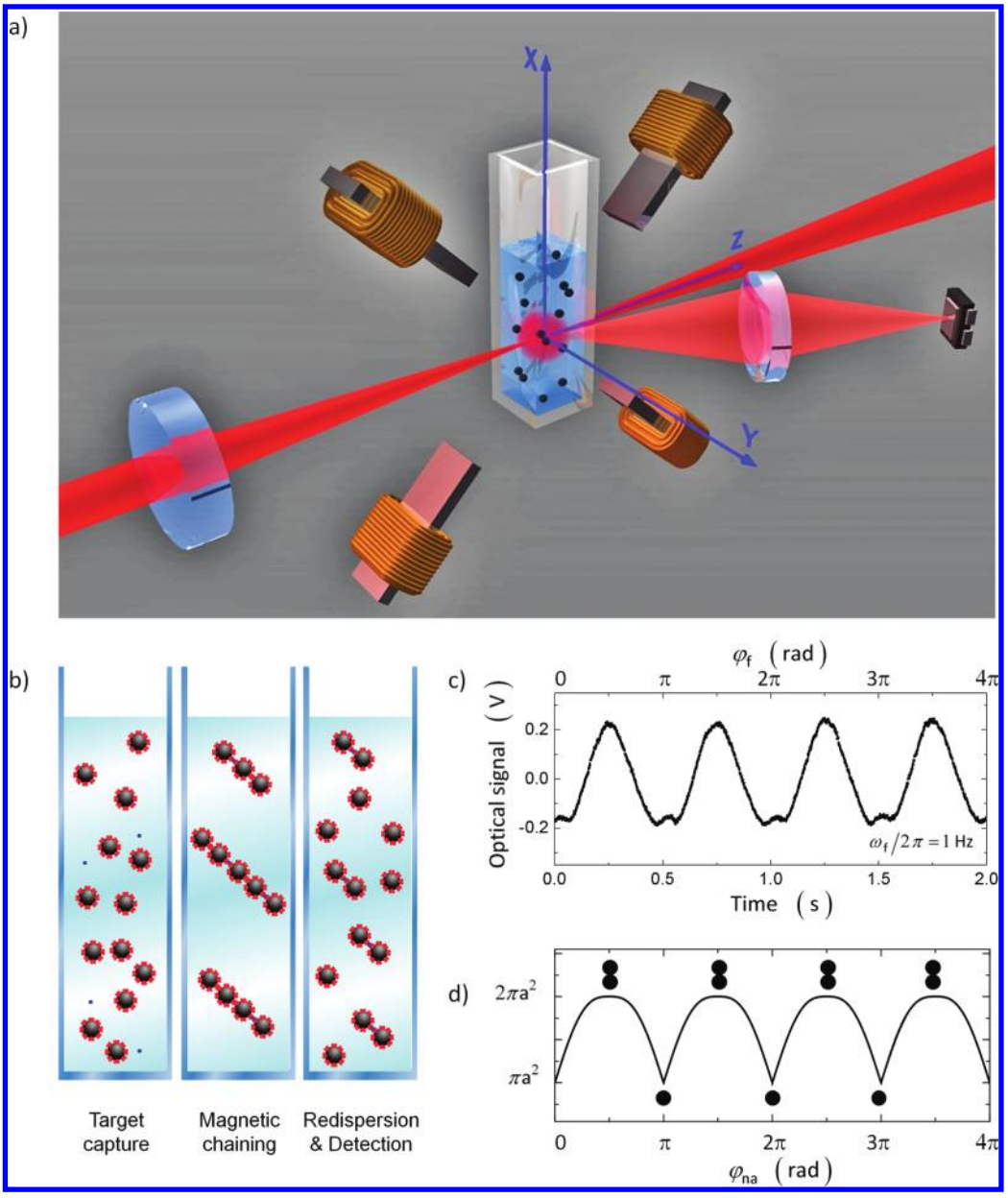

Figure 1. The opto-magnetic system and nanoparticle assay. Panel a sketches the optomagnetic platform used in our experiments. A collimated laser beam is focused at the center of four electromagnets where a glass cuvette is placed. The light scattered at an angle of approximately 30° with respect to the incoming laser beam is focused onto a photodetector. Panel b shows the three phases of the biological assay. First, biologically activated nanoparticles are incubated with the target proteins. Thereafter a rotating magnetic field is applied to drive the formation of nanoparticle chains, which enables effective internanoparticle binding. Finally, the magnetic field is removed to allow unbound nanoparticles to redisperse, and the optical scattering is detected under frequency-selective magnetic actuation. Panel c shows the typical optical scattering signal measured from two-particle nanoactuators in a magnetic field rotating at 1 Hz. Panel d shows the calculated geometrical cross-section of a two-particle nanoactuator during the rotation.

disassemble. Finally, a rotating magnetic field is applied that selectively actuates the nanoactuators for detection.

The sensitive and selective detection of two-particle nanoactuators embedded in an ensemble of single nanoparticles is based on two distinguishing features, namely magnetic anisotropy and optical anisotropy. The magnetic shape anisotropy of a two-particle nanoactuator enables frequency-controlled rotation,[14] while the optical anisotropy of a nanoactuator generates a modulation of optically scattered light. Single particles contribute negligibly to the optical modulation because they lack the characteristic magnetic and optical anisotropies of the two-particle nanoactuators. Figure 1c shows the measured optical scattering of nanoactuators in a field of $\mu_0 H = 3.5$ mT rotating at a frequency $\omega_f/2\pi = 1$ Hz. We observe that the signal period equals half the period of the applied field. This is a direct consequence of the equivalence of individual particles and the resulting point symmetry of a two-particle nanoactuator. The data show that scattering is highest when the nanoactuators are aligned perpendicular to the optical beam, that is, when they expose their largest geometrical cross-section toward the incoming light beam. The orientations of lowest signal are close to an orientation along the optical beam. Figure 1d shows the

dx.doi.org/10.1021/nl200384p |*Nano Lett.* 2011, 11, 2017–2022

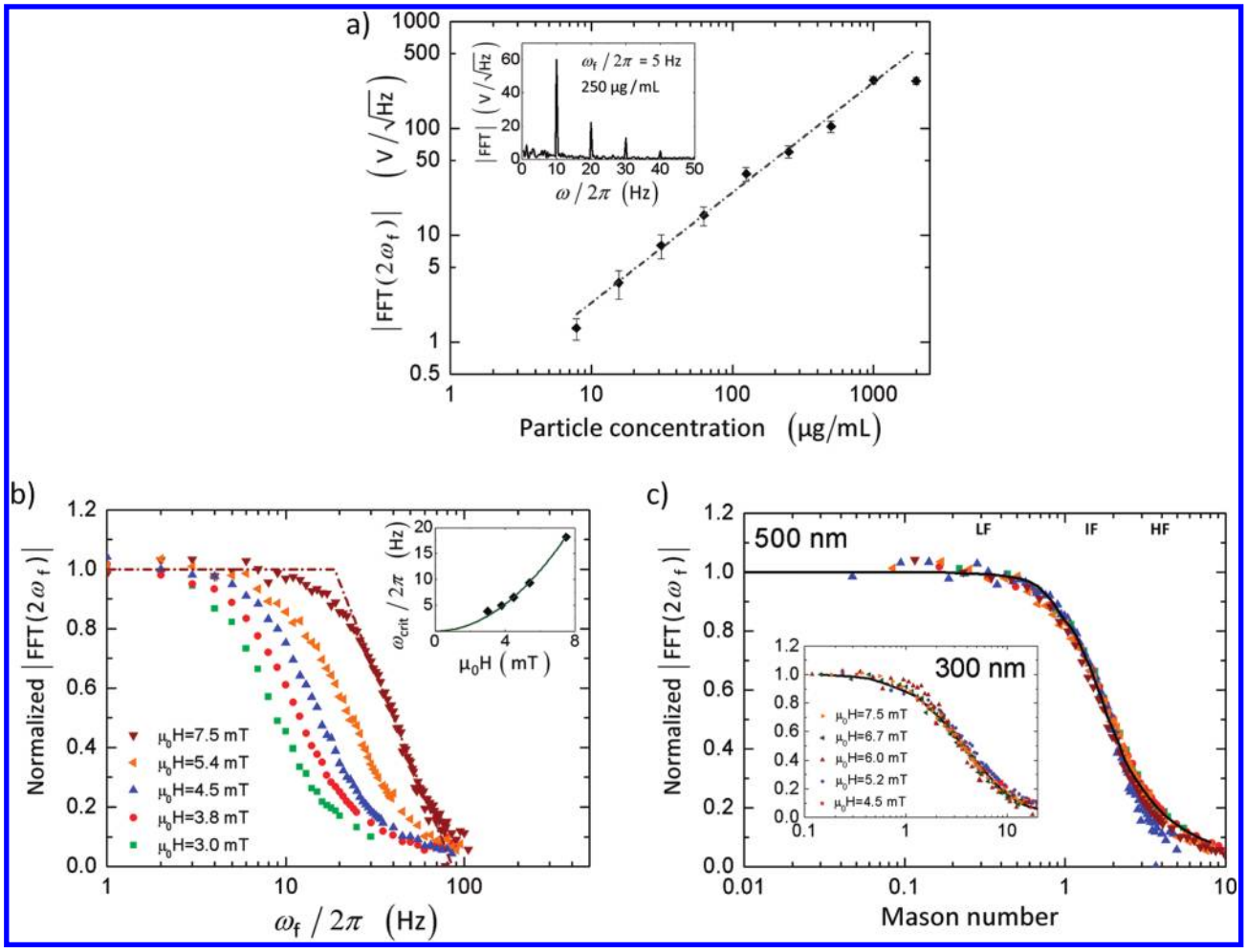

Figure 2. Optical scattering signal as a function of particle concentration and magnetic field properties. The ratio of two-particle nanoactuators to single particles is about 1:20. The linear behavior in panel a shows that the signal is proportional to the number of nanoactuators present in the sample and allows us to estimate the signal per two-particle nanoactuator. The inset shows the Fourier transform of the signal measured at a particle concentration of 250 μg/mL and a field frequency of 5 Hz. Panel b shows the frequency dependent response of particles with a diameter of 500 nm for several values of the strength of the magnetic field. The crossing point of the linear fits at low and intermediate frequencies gives the value of the critical frequency (the lines are shown for the measurement at 7.5 mT). The inset shows the value of the critical frequency as a function of the magnetic field strength; the quadratic fit demonstrates that the dipole−dipole interaction is the main source of the magnetic torque. Panel c shows the same data as in Figure 3b, but now the data is plotted as a function of the dimensionless Mason number. The low frequency (LF), intermediate frequency (IF), and high frequency (HF) zones are indicated. To fit the data, we numerically solved eq 1 for an ensemble of 100 nanoactuators with a normal distribution of volume susceptibility. The mean value of the distribution was chosen to equal the average value obtained by the measurements of critical frequency shown in the inset of Figure 2b; the standard deviation was varied to best fit the experimental data by minimizing the mean square error. The data of the 500 nm diameter Masterbeads give a volume susceptibility of 2.4 ± 0.8. The data of the 300 nm diameter Bioadembeads (see inset) give a volume susceptibility of 2.0 ± 0.9.

calculated geometrical cross-sectional area as a function of φ_{na}, the angle of the nanoactuator axis to the z-axis, for a nanoactuator that consists of two nanoparticles with radius a. The geometrical cross-sectional area reproduces the half-period characteristic and has the same phase as the optical scattering signal, but the shapes of the curves are quite distinct. For example, the measured scattering curve shows interesting subtle features when the nanoactuators are nearly aligned along the optical beam ($\varphi_{na} \sim n\pi$). We attribute such features to the angle-dependent nature of the differential scattering cross section $\sigma_{na}(\vartheta,\varphi)$ of the nanoactuators,[15,16] a topic that we will address in further research.

To calibrate the optomagnetic detection system, we performed experiments for different solution concentrations (see Figure 2a). A stock solution was diluted to a particle concentration of 2 mg/mL and sonicated, leading to a solution with many single nanoparticles and a low number of two-particle nanoactuators. The composition of the calibration sample was quantified by optical microscopy, showing a 1:20 ratio of two-particle nanoactuators to single nanoparticles. Clusters of larger size were not observed. The recorded curves of optical signal as a function of time were analyzed by an FFT algorithm (fast Fourier transform) with an integration time of 3 s. The FFT spectrum (see inset) shows only even harmonics, as expected from the point symmetry of the nanoactuators. The peak at 2f dominates the spectrum. The magnitude of the 2f peak shows a linear dependence on the particle concentration with a dynamic range of about two decades. From the slope of the curve, the known concentration of two-particle nanoactuators in the solution, and the optical probing volume in our system (about 1 nL), we deduce a value of 0.7 V/(Hz)$^{1/2}$ for the optical signal per two-particle nanoactuator in our setup.

dx.doi.org/10.1021/nl200384p |*Nano Lett.* 2011, 11, 2017–2022

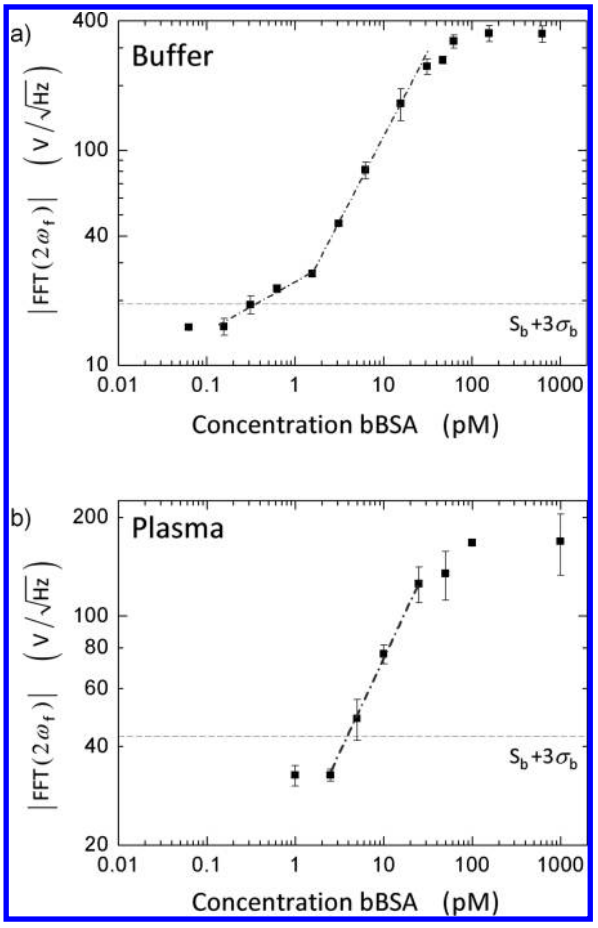

Figure 3. Dose−response curves for assays in buffer (panel a) and in plasma (panel b). For every measurement point, a frequency scan was performed as in Figure 2b, measured for a field magnitude of 3.5 mT. The signal corresponds to the low-frequency plateau value (1 to 5 Hz) of the 2f signal of the FFT spectrum. The dashed lines are guides to the eye. In panel a, the final nanoparticle concentration was 85 μg/mL. The signal level at low concentrations corresponds to approximately 20 two-particle nanoactuators in the optically probed volume. The dashed lines show two slopes which reflect the nanoactuator size distribution, as is further detailed in Figure 4. In panel b, the final particle concentration was 55 μg/mL; the signal at low concentrations corresponds to the presence of roughly 50 two-particle nanoactuators in the probing volume. We attribute the higher blank values in plasma compared to buffer to the presence of interfering agents in the complex matrix. The gray lines in both panels represent the value of $S_b + 3\sigma_b$ that is, the blank plus three times the σ of the blank.

Our system allows a detailed characterization of the magnetic properties of the nanoactuators. In a recent paper,[14] we have developed the equation of motion for a single two-particle actuator in a rotating magnetic field. In the low-frequency regime, the nanoactuators rotate synchronously with the applied field. At a critical frequency, the phase difference between the applied field and the magnetic moment is maximum, so a maximum torque is applied and a maximum rotation frequency is realized. Beyond the critical frequency, the rotation shows a wiggling behavior in which forward and backward motions alternatingly appear. The backward rotations reduce the net forward angular velocity, an effect that becomes stronger for increasing frequency of the external field. When magnetic shape anisotropy dominantly generates the magnetic torque, the equation describing the motion of a two-particle nanoactuator in a uniform magnetic field $\vec{H}$ rotating in the xz plane at frequency ω_f is given by

$$\frac{d\varphi_{na}}{dt} = \omega_{crit} \sin[2(\varphi_i - \varphi_{na})] \quad \text{with}$$

$$\sin(\varphi_i - \omega_f t) + \frac{\chi}{16} \sin[2(\varphi_i - \varphi_{na})] = 0 \qquad (1)$$

where $\omega_{crit} = \mu_0 \chi^2 H^2 / 168\eta$ represents the value of the critical frequency, φ_i is the angle between the direction of the induced magnetic moment and the z-axis, φ_{na} is the angle between the axis of cylindrical symmetry of the nanoactuator and the z-axis, μ_0 is the magnetic permeability of vacuum, χ is the dimensionless volume susceptibility of the magnetic nanoparticle material, and η is the viscosity of the fluid medium. The equations are derived by balancing the magnetic and viscous torques. The equations are independent of the size of the nanoparticles because the magnetic and viscous torques both scale with the volume of the particles; this means that our actuation method is in principle applicable to a wide range of particle sizes.

Figure 2b shows the frequency-dependence of rotation of the nanoactuators for different magnitudes of the applied magnetic field, measured on a mixture of two-particle nanoactuators and single particles. In the low-frequency regime, the signal is independent of frequency since the nanoactuators rotate synchronously with the applied field. At intermediate frequencies, a gradual decrease of signal is observed. We attribute the signal decrease to a progressive diminishment of the number of two-particle nanoactuators that is able to rotate synchronously with the magnetic field. A spread in size and magnetic content in the nanoparticles results in a distribution of critical frequencies; the nanoactuators with the lowest volume susceptibility are the first to deviate from the synchronous rotation and at higher frequencies more and more nanoactuators enter the regime of wiggling rotation. In the wiggling regime, the amplitude of the 2f modulation decreases and FFT signals appear at lower frequencies. We determined the critical frequency from the point where the intermediate frequency curve extrapolates to unity, as indicated in Figure 2b. The inset shows the measured critical frequency as a function of the applied field; the observed quadratic dependence proves that the magnetic shape anisotropy of the nanoactuators is at the origin of the rotation.

The data can also be expressed as a function of a dimensionless parameter, the Mason number, which represents the ratio between viscous and magnetic torque[14]

$$\mathrm{Mn} = \frac{168\eta\omega}{\mu_0 \chi^2 H^2} \qquad (2)$$

At the critical frequency (see eq 1) the Mason number equals unity. In Figure 2c, the data for nanoparticles with a diameter of 300 and 500 nm are plotted as a function of the Mason number. The measurement points collapse into a single curve that is specific for the type of particle. We have modeled the curves by summing responses for an assumed normal distribution of susceptibility values. For the 500 nm particles, a good curve fit is found with $\chi = 2.4 \pm 0.8$, which is in agreement with the value of 2.65 found by vibrating sample magnetometry (VSM). For the 300 nm particles, the curve fit yields $\chi = 2.0 \pm 0.9$, which

dx.doi.org/10.1021/nl200384p |*Nano Lett.* 2011, 11, 2017–2022

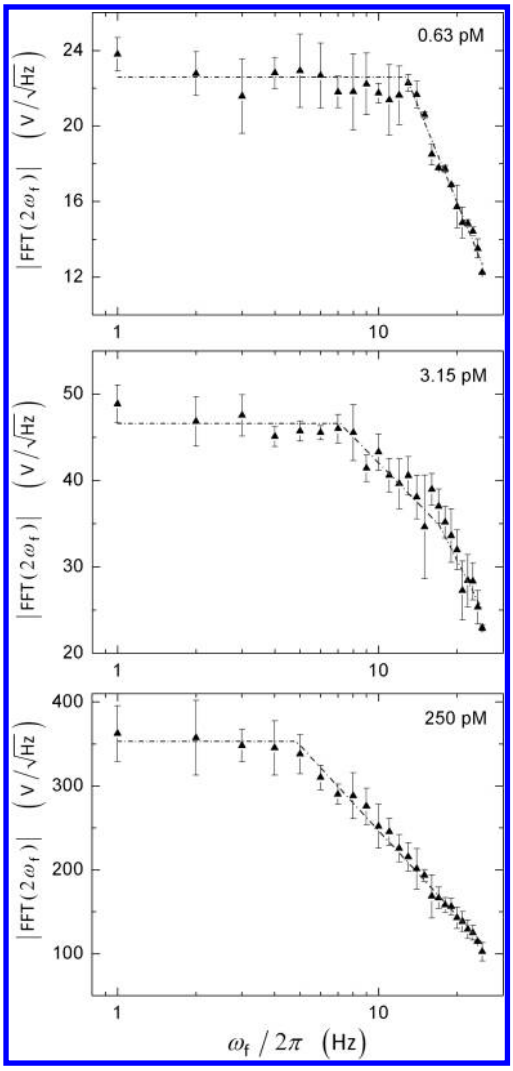

Figure 4. Frequency response for three concentrations of bBSA in buffer (0.63 pM in top panel, 3.15 pM in middle panel, and 250 pM in bottom panel). The measurements were performed in a field of 3.5 mT with an averaging time of 3 s. The critical frequency shifts to lower values for increasing bBSA concentrations due to the presence of nanoactuators of increasing size. The signal at low frequencies increases with the concentration of bBSA because of the larger size and number of nanoactuators. The dotted lines are obtained by fitting the experimental points and are used to estimate the critical frequencies. The data at a concentration of 3.15 pM show the copresence of nanoactuators made of three and two nanoparticles, respectively, characterized by a critical frequency of approximately $\omega_{crit}/2\pi = 7$ and 16 Hz. At the latter critical frequency, the slope of the frequency dependent signal doubles.

compares well with the VSM value of 2.15 and with data from confined Brownian motion analysis.[17]

In the above experiments, we have demonstrated that optical scattering is an accurate tool to characterize the rotational dynamics of an ensemble of two-particle nanoactuators and that the amplitude of the 2f signal is an accurate measure for the amount of nanoactuators in the sample. We proceed by investigating assays as in Figure 1b, using strepavidin-coated magnetic nanoparticles and biotinylated BSA (bBSA) as target molecule. A 6 μL sample of magnetic nanoparticles and bBSA is incubated for 10 s. The sample undergoes magnetic chaining for 2 min and is then diluted to tune the signal from the nanoparticles to the dynamic range of the photodetector and to avoid potential cluster growth during the subsequent detection phase. Detection is performed under frequency-selective magnetic actuation. Further details are given in the Supporting Information.

Figure 3 shows dose−response curves for assays in buffer and in plasma. The optomagnetic signal clearly increases as a function of the target concentration. Interestingly, the dose−response curve in buffer shows two distinct slopes, sketched with dotted lines in the figure. We attribute the change of slope to a transition in the size distribution of the nanoactuators. The size distribution depends on the ratio of the number of bBSA molecules to the number of nanoparticles. During incubation, the nanoparticle concentration is approximately 10 pM. So at target concentrations below 2 pM only two-particle nanoactuators are statistically likely to form. When the number of bBSA molecules increases and becomes comparable to the number of nanoparticles, the probability increases that nanoactuators consist of more than two nanoparticles. To further investigate the concentration dependence, we measured frequency response curves for three concentrations of bBSA, as shown in Figure 4. The critical frequency is derived from the crossing between the fits at low and intermediate frequencies. The critical frequency is about 13 Hz for a target concentration of 0.6 pM, reduces to 7 Hz for 3.1 pM, and becomes 4.8 Hz for 250 pM. In fact, the curve at 3.1 pM shows two critical transitions with increasing slope steepness. We attribute the two slopes at 3.1 pM to the contemporary presence of comparable quantities of two-particle and three-particle nanoactuators. The dependence of the critical frequency on the number of particles in a nanoactuator has been theoretically investigated[18] and it is in agreement with our results. The low-frequency concentration-dependent signals lead to a dose−response curve as in Figure 3a. The detection limit, defined as the level where the signal equals $S_b + 3\sigma_b$, with S_b as the average of the blank signal and σ_b as the standard deviation of the blank signal, is found to be below 400 fM. The detection limit is determined by nonspecific binding processes of the nanoparticles. The signal saturates at a target concentration of about 100 pM, caused by the limited number of nanoparticles that is available for nanoactuator formation.

Analytical assays are particularly challenging in complex biological matrices such as blood plasma, due to the large quantities of potentially interfering molecules.[19] Figure 3b shows a dose−response curve measured in human plasma. The optical signal increases with the concentration of bBSA and reaches saturation at a value of approximately 100 pM. A transition of slope, as is observed in buffer, is not seen in plasma. The reason is that the blank levels are higher in plasma, due to the presence of interfering agents that generate nonspecific binding between nanoparticles. The blank level has variations of about 13%, which gives a value close to 5 pM as the limit of detection. To our knowledge, this is the first literature report of a dose−response curve with low-picomolar protein detection in undiluted plasma for an all-volume-based cluster assay using magnetic nanoparticles.

In this Letter, we have demonstrated an optomagnetic technology that is suited to characterize nanoparticle properties and to sensitively and rapidly detect biological molecules in a very small sample volume. A measurement of the frequency response reveals the magnetic properties, concentration, and size distribution of nanoactuators in the sample. Frequency-selective nanoactuator rotation provides a baseline-free detection technique for solution-based biological assays in buffer and in human plasma. We have demonstrated a limit of detection of 400 fM in buffer

dx.doi.org/10.1021/nl200384p |*Nano Lett.* 2011, 11, 2017–2022

and 5 pM in plasma, in a total assay time of less than 3 min. The platform integrates two bio-orthogonal principles, namely magnetic actuation and optical detection, allowing for independent tuning of the experimental parameters. In the optical domain, the technology holds promise for further studies of the angle-dependent scattering properties of magnetic nanoparticles with high accuracy due to magnetic control of orientation and the possibility to average signals over several revolutions. In the field of colloid interactions, the technology will enable studies of the kinetics of colloidal interactions for a wide variety of systems, for example, nanoparticles with different surface chemistries and in different matrices. Furthermore, the volume-invariance of the rotation dynamics (see eq 1) allows an extrapolation of the method toward smaller sizes of nanoparticles. The use of smaller particles will allow the characterization of novel nanoparticle materials, studies of their aggregation properties, as well as studies of all-volume-based biological assays with high nanoparticle concentrations and high assay kinetics. In summary, we have presented an innovative and versatile optomagnetic bionanotechnology that paves the way for a wide range of nanotechnological and biochemical studies.

■ ASSOCIATED CONTENT

Supporting Information. Additional information. This material is available free of charge via the Internet at http://pubs.acs.org.

■ AUTHOR INFORMATION

Corresponding Author

*E-mail: menno.prins@philips.com. Telephone: +31 40 27 48497. Fax: +31 40 27 42944.

■ ACKNOWLEDGMENT

This work was partially funded by The Netherlands Ministry of Economic Affairs via the MicroNed programme.

■ REFERENCES

(1) Yager, P.; Edwards, T.; Fu, E.; Helton, K.; Nelson, K.; Tam, M. R.; Weigl, B. H. *Nature* **2006**, *442* (7101), 412–418.

(2) Stern, E.; Vacic, A.; Rajan, N. K.; Criscione, J. M.; Park, J.; Ilic, B. R.; Mooney, D. J.; Reed, M. A.; Fahmy, T. M. *Nat. Nanotechnol.* **2010**, *5* (2), 138–142.

(3) Fan, R.; Vermesh, O.; Srivastava, A.; Yen, B. K. H.; Qin, L.; Ahmad, H.; Kwong, G. A.; Liu, C. C.; Gould, J.; Hood, L. *Nat. Biotechnol.* **2008**, *26* (12), 1373–1378.

(4) Bruls, D. M.; Evers, T. H.; Kahlman, J. A. H.; Lankvelt, P. J. W.; Ovsyanko, M.; Pelssers, E. G. M.; Schleipen, J. J. H. B.; Theije, F. K.; Verschuren, C. A.; van der Wijk, T.; Van Zon, J. B. A.; Dittmer, W. U.; Immink, A. H. J.; Nieuwenhuis, J. H.; Prins, M. W. J. *Lab Chip* **2009**, *9* (24), 3504–3510.

(5) Wild, D. *The immunoassay handbook*; Elsevier Science Ltd: New York, 2005.

(6) Handorf, C. R. *Clin. Chim. Acta* **1997**, *260* (2), 207–216.

(7) Luchini, A.; Geho, D. H.; Bishop, B.; Tran, D.; Xia, C.; Dufour, R. L.; Jones, C. D.; Espina, V.; Patanarut, A.; Zhou, W.; Ross, M. M.; Tessitore, A.; Petricoin, E. F.; Liotta, L. A. *Nano Lett.* **2008**, *8* (1), 350–361.

(8) Seydack, M. *Biosens. Bioelectron.* **2005**, *20* (12), 2454–2469.

(9) Fornara, A.; Johansson, P.; Petersson, K.; Gustafsson, S.; Qin, J.; Olsson, E.; Ilver, D.; Krozer, A.; Muhammed, M.; Johansson, C. *Nano Lett* **2008**, *8* (10), 3423–3428.

(10) Baudry, J.; Rouzeau, C.; Goubault, C.; Robic, C.; Cohen-Tannoudji, L.; Koenig, A.; Bertrand, E.; Bibette, J. *Proc. Natl. Acad. Sci. U.S.A.* **2006**, *103* (44), 16076.

(11) Moser, Y.; Lehnert, T.; Gijs, M. A. M. *Lab Chip* **2009**, *9* (22), 3261–3267.

(12) Park, S. Y.; Handa, H.; Sandhu, A. *Nano Lett.* **2010**, *10* (2), 446–451.

(13) Koh, I.; Hong, R.; Weissleder, R.; Josephson, L. *Angew. Chem., Int. Ed.* **2008**, *47* (22), 4119–4121.

(14) Ranzoni, A.; Janssen, X. J. A.; Ovsyanko, M.; IJzendoorn, L. J.; Prins, M. W. J. *Lab Chip* **2010**, *10* (2), 179–188.

(15) Gerardy, J. M.; Ausloos, M. *Phys. Rev. B* **1982**, *25* (6), 4204.

(16) Quinten, M.; Kreibig, U. *Appl. Opt.* **1993**, *32* (30), 6173–6182.

(17) van Ommering, K.; Nieuwenhuis, J. H.; van IJzendoorn, L. J.; Koopmans, B.; Prins, M. W. J. *Appl. Phys. Lett.* **2006**, *89* (14), 3.

(18) Petousis, I.; Homburg, E.; Derks, R.; Dietzel, A. *Lab Chip* **2007**, *7* (12), 1746–1751.

(19) Gaster, R. S.; Hall, D. A.; Nielsen, C. H.; Osterfeld, S. J.; Yu, H.; Mach, K. E.; Wilson, R. J.; Murmann, B.; Liao, J. C.; Gambhir, S. S. *Nat. Med.* **2009**, *15*, 1327–1332.